Image Synthesisation and Data Augmentation for Safe Object Detection in Aircraft Auto-landing System

Najda Vidimlic, Alexandra Levin, Mohammad Loni and Masoud Daneshtalab
School of Innovation, Design and Engineering, Mälardalen University, Västerås, Sweden

Keywords: Object Detection, Data Augmentation, Synthesised Image, Safety, Situational Awareness.

Abstract: The feasibility of deploying object detection to interpret the environment is questioned in several mission-critical applications leading to raised concerns about the ability of object detectors in providing reliable and safe predictions of the operational environment, regardless of weather and light conditions. The lack of a comprehensive dataset, which causes class imbalance and detection difficulties of hard examples, is one of the main reasons of accuracy loss in attitude safe object detection. Data augmentation, as an implicit regularisation technique, has been shown to significantly improve object detection by increasing both the diversity and the size of the training dataset. Despite the success of data augmentation in various computer vision tasks, applying data augmentation techniques to improve safety has not been sufficiently addressed in the literature. In this paper, we leverage a set of data augmentation techniques to improve the safety of object detection. The aircraft in-flight image data is used to evaluate the feasibility of our proposed solution in real-world safety-required scenarios. To achieve our goal, we first generate a training dataset by synthesising the images collected from in-flight recordings. Next, we augment the generated dataset to cover real weather and lighting changes. Introduction of artificially produced distortions is also known as corruptions and has since recently been an approach to enrich the dataset. The introduction of corruptions, as augmentations of weather and luminance in combination with the introduction of artificial artefacts, is done as an approach to achieve a comprehensive representation of an aircraft's operational environment. Finally, we evaluate the impact of data augmentation on the studied dataset. Faster R-CNN with ResNet-50-FPN was used as an object detector for the experiments. An AP@[IoU=.5:.95] score of 50.327% was achieved with the initial setup, while exposure to altered weather and lighting conditions yielded an 18.1% decrease. The introduction of the conditions into the training set led to a 15.6% increase in comparison to the score achieved from exposure to the conditions.

1 INTRODUCTION

Object detection is a versatile technology which is used to solve complex vision tasks, such as face detection in smartphones (Dave et al., 2010), path planning and obstacle avoidance for robots (Engelcke et al., 2017; Ball et al., 2016), surveillance applications in cities (Alam et al., 2020; Geng et al., 2018), and visual auto-landing of an aircraft (Zhang et al., 2019).

The performance of the object detector is not only dependent on the usage of appropriate hardware and the available computing capabilities to efficiently solve the task. Knowledge of the applications' operational environment and the objects-in-context determines the performance of the object detector. The feasibility of deploying object detection to interpret the environment is questioned in several industries and concerns are raised about the object detector applications' ability to provide reliable and safe predictions of the operational environment, regardless of environmental conditions. In the automotive industry, object detection has been deployed as a mean to detect and locate pedestrians, traffic signs, and obstacles to enable autonomous driving (Badue et al., 2019). However, challenges persist in the object detection domain and were further questioned when a Tesla car operating in autonomous mode crashed into a truck due to inability of the object detection system to distinguish between a white truck and the sky (J.Steward, 2018).

Deploying vision-based object detection in aviation imposes rigorous challenges since it is one of the most stringent industries, and thus, development is strictly regulated to ensure system safety. In situations of reduced visibility or cluttered environments, enhanced vision through object detection could aid a pilot in environment interpretation and improve detection of hazardous objects. The operational environment of an aircraft during the landing phase has

Vidimlic, N., Levin, A., Loni, M. and Daneshtalab, M.
Image Synthesisation and Data Augmentation for Safe Object Detection in Aircraft Auto-landing System.
DOI: 10.5220/0010248801230135
In *Proceedings of the 16th International Joint Conference on Computer Vision, Imaging and Computer Graphics Theory and Applications (VISIGRAPP 2021) - Volume 5: VISAPP*, pages 123-135
ISBN: 978-989-758-488-6

several, both dynamic and static, objects to consider, and a particular challenge is to assess if a certain object could impose a hazardous situation.

The International civil aviation organization (ICAO) identifies the runway safety-related events (such as bird strike, ground collision, collision with an obstacle(s), runway incursion, runway excursion, etc.) as the majority of flight accidents in 2018 with contributing 48% of all accidents and 70% of accidents with aircraft substantially damaged or destroyed (ICAO, 2019). Besides, according to the statistics on aviation accidents report provided by the International Air Transport Association (IATA) in 2019 (Association et al., 2019), the low visibility, meteorology, and visual misperception are accounted for 16%, 56%, and 6% of runway safety threats, respectively. Thus, the importance of safe object detection during the aircraft landing phase is evident (Skybrary, 2017).

Through vision-based object detection, accidents could possibly be avoided. Proving safe detection of hazardous objects in aviation is heavily reliant on broad and diverse data about the operational environment to ensure consistent and accurate detection. To ensure the environment is correctly represented, a comprehensive and robust data representation which includes various objects, both dynamic and static, as well as weather and lighting variations, is highly essential. However, collecting large-scale comprehensive image samples to provide the model with more information about the learning pattern is extraordinarily laborious and resource-demanding. Thus, constructing a diverse and robust representation of the environment of aircraft landing operation using data augmentation techniques is the goal of this paper. Our contributions can be summarised as follows:

- Construction of a robust runway detection dataset to ensure continuous environment interpretation during aircraft landing operation, regardless of weather and lighting changes.
- Manual image synthesis to ensure diverse object representation of the operational environment in the dataset.
- Applying common data augmentation techniques including geometric/photometric transformations, random erasing, sample pairing, etc., to increase the size of dataset.
- Applying weather and lighting augmentations to enrich dataset and ensure robust object detection, regardless of environmental changes.
- Measuring the number of artificial artefacts with respect to un-distorted images to ensure context-awareness throughout the dataset.
- Defining an experimental method to compare detection results by considering three scenarios. In our experiments, we utilised Faster R-CNN with three different backbones (ResNeXt-101-FPN, ResNet-101-FPN, and ResNet-50-FPN) as the object detector due to providing high localisation accuracy of small objects (Levin and Vidimlic, 2020; **?**) (Section 5.1)
- As illustrated in Fig. 1, the proposed safety method improves the accuracy of object detection in situations with bad weather.

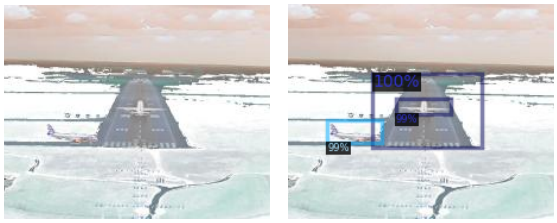

(*a*) (*b*)

Figure 1: Comparison of object detection capabilities between one output result without weather and lighting augmentations in training dataset and one with. The input image shows a snowy landscape. (a) Output results trained without weather and lighting augmentations. (b) Output results of successful detection trained with data augmentation.

2 BACKGROUND

The interpretation of the operational environment during all stages of flight is the pilot's outermost task. The correct interpretation is crucial for airborne safety and part of situational awareness. To visualize the environment, two primary information sources are available. The first is provided by visual interpretation, and the second is provided by navigation-, safety-, and decision support systems. Support systems such as Automatic Dependent Surveillance-Broadcast (ADS-B), Traffic Collision Avoidance System (TCAS) and Terrain Avoidance and Warning System (TAWS) that provide knowledge of terrain height, as well as the position of ground-based and airborne objects that are in close proximity, could highly reduce the risk of collision (Federal Aviation Administration, 2017; **?**). Applying object detection to interpret, detect and track potentially hazardous objects in the aircraft's proximity could provide the necessary means further to reduce the risk of hazardous situations within aircraft operations and enhance the situational awareness for the pilot or perform auto-landing functions.

Recently, deep learning became a very popular tool for performing computer vision tasks due to

yielding higher accuracy, training on any desired input space, and the ease of usability in comparison with conventional methods (O'Mahony et al., 2019; Loni et al., 2020).

2.1 Importance of the Dataset

The object detector's performance is highly dependent on the training data, which is a fundamental part of the ability to perform meaningful feature extraction in neural networks (NNs). The model could only be as good as the data it is trained on. The required amount of data to build a sufficient prediction model is dependent on the prediction task complexity. In general, a comprehensive dataset provides the model with more information about the learning pattern and could yield predictions with higher correctness and accuracy (Shorten and Khoshgoftaar, 2019). A comprehensive dataset would need to be both qualitative and quantitative, including a large amount of data as well as varying data over the prediction classes. However, acquiring a comprehensive dataset is an extensive task, or sometimes impossible, which includes the collection, pre-processing, and annotation steps. To speed up the development, open-source benchmark dataset are publicly available to use for object detection tasks (Mitsa, 2019), such as MS-COCO (Lin et al., 2014), Pascal VOC (Everingham et al., 2010), and ImageNet (Deng et al., 2009). In this paper, we construct a robust runway detection dataset by combining in-flight recordings and further extend the dataset by using royalty-free images with relevant motifs (Section 4).

2.2 Deep Learning Safety Issues

Faria (Faria, 2017) states that the system property determinism is of great importance for the certification of safety-critical software. Safety-related activities require indirect evidence of determinism, providing predictability and in-depth understanding of the software. S. Burton et al. (Burton et al., 2017) discuss the challenges of providing evidence for the safety case and identified measurable performance criterion; transparency, environment adaption and dataset comprehension to be the critical building blocks affecting the safety case. Producing test cases for validation of the applications ability to provide a safe trajectory in the case of exposure of harmful objects on a runway could be challenging since the test cases need to cover a wide range of scenarios to provide evidence to support claims of acceptably safe. Moreover, the transparent nature of deep learning algorithms affects the safety and predictability throughout execution needs to be ensured. Furthermore, S. Burton et al. (Burton et al., 2017) discusses the importance of the constructed dataset of the operational environment and the impact of details to ensure safety. The context is of extreme importance to provide safe interpretation. For example, given a dataset constructed with a camera lens in a titling-angle, the application in operation would need to be utilised with the corresponding setup. Also, the constructed dataset needs to be comprehensive and cover scenarios that describe the operational environment to a vast extent, without imposing hazardous situation while building the representation by placing hazardous objects on the airport runway in during the real flight operations. Accordingly, each of the mentioned parameters need to be considered, and the outcome of each input needs to be known to deploy deep learning applications in safety-critical systems safely.

3 RELATED WORK

To the best our knowledge, this paper presents the first attempt toward *safety* enhancement of visual detection system via data augmentation. To guarantee safety, hazards must be mitigated until an acceptable level of risk is achieved. By utilising artificial intelligence, new hazards are introduced, and thus higher demands are placed upon the performance of the introduced parts. NNs are evaluated by their generalisation performance, how well the models are able to adapt to new unseen data. Techniques enhancing generalisation performances of NNs are incorporated into various architectures with the aim to produce the most optimal model. In addition to the architecture, the scope and diversity of a dataset greatly inflict upon the generated model's generalisation capability. To vary structure, objects, and depiction, as well as to increase the size and scope of the dataset, multiple data augmentation techniques have been proposed over the years. Data augmentation techniques include all modifications of images, including light manipulations such as flipping, cropping, and contrast alterations.

3.1 Common Data Augmentation Techniques

C. Shorten and T.M. Khoshgoftaar (Shorten and Khoshgoftaar, 2019) describes common used augmentation techniques. The different techniques can be divided into five categories; geometric transformation, photometric transformation, kernel filters, random erasing, and sample-pairing, where geometric

transformation, photometric transformation, and kernel filters acts as umbrella terms as seen in Fig. 2.

Basal augmentations techniques, such as axis flipping, cropping, rotation, and RGB colour space alterations are covered by the first umbrella term, geometric transformation. The term also covers translations, shifting an object's position within an image up, down, left or right, and noise injection, alteration of pixel values by random values. The second umbrella term, photometric transformation, covers techniques focusing on alteration of specific pixels, including jittering, edge enhancement, and Principal Component Analysis (PCA). The first method induces fixed or random values to the pixel values which temporary distorts the image, while the second method targets and characterises the pixel edges of interesting objects (Taylor and Nitschke, 2017). PCA Color Augmentation is a method introduced in conjunction with the creation of AlexNet in 2012; the method aims to identify which RGB colour is most prominent in the image and thereafter adjust the pixel values according to the intensity. Kernel filters, the third umbrella term, includes Gaussian blur, vertical edge, and horizontal edge filters. Vertical and horizontal edge filters increase the sharpness of an image, while Gaussian blur reduces the sharpness (Shorten and Khoshgoftaar, 2019).

3.2 Data Augmentation to Improve Accuracy

As a supplement to the well-known augmentation techniques, several other data augmentation techniques have been proposed to increase the accuracy and enhance the generalisation performance. The method Random erasing was presented in 2017 by (Zhong et al., 2017), followed by SamplePairing in 2018 by (Inoue, 2018). The first method randomly selects a rectangular area within the image, where a new randomly generated value modifies each pixel. By removing fractions of information from images of the dataset, the model may achieve higher robustness towards loss of information. SamplePairing, on the other hand, creates a new image by using two images, A and B, with two labels, A and B. Each pixel of the new image is created by taking the average pixel value of the corresponding pixel values of images A and B. The new image is labelled according to label A, regardless of image results. (Inoue, 2018) reported a varied reduction of training and validation error depending on how image B was collected. Collecting image B without any constraints from the training set achieved the most superior results.

L.A. Gatys et al. (Gatys et al., 2015) introduced a more artistic inspired technique, known as style transfer. The method utilises two images, an input image and a style image, to create a new image with features of the input image yet influenced by the shapes and colours of the style image. Style transfer was then used by R. Geirhos et al. (Geirhos et al., 2018) to investigate the importance of texture and shape for object recognition. Results were unexpected and contradicted what had previously been assumed; object detectors tended to learn based on textures of objects rather than the object shape (Geirhos et al., 2018).

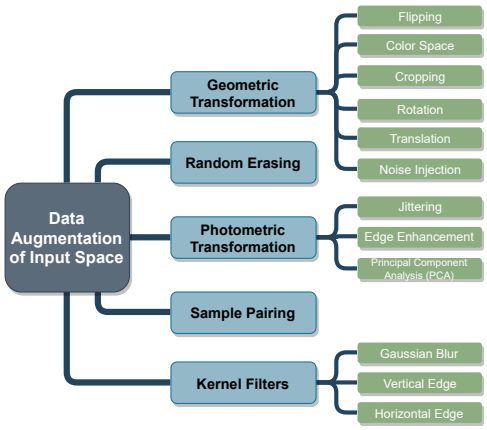

Figure 2: A visualisation of augmentation technique classes.

Distortion within data augmentation received increased attention, not only distortion of texture by style augmentation but also by including natural distortions such as snow, rain, fog, and clouds within the images. Introduction of artificially produced distortions is also known as corruptions and has since recently been an approach to enrich the dataset in addition to the earlier discussed augmentation techniques. Hendrycks and Dietterich (Hendrycks and Dietterich, 2018) performed an experiment to evaluate the impact of introducing corruptions to the test set; 15 corruption methods were applied in total to conduct the experiment. Each corruption method had five intensity levels, which resulted in 75 different scenarios. For the experiment, various NN models were trained on data from ImageNet. Their results revealed the robustness capabilities of each trained model, indicating DenseNet and ResNeXt to be the best models.

Three additional corruption datasets were created by Michaelis et al. (Michaelis et al., 2019) by imitating the experiment of Hendrycks and Dietterich, creating Pascal-C, Coco-C, and Cityscape-C. Further, as the second test in addition to the reconstructed experiment, style augmented images were introduced during training. The results pointed towards increased robustness capabilities without compromising the object detection capability of corruption-free images.

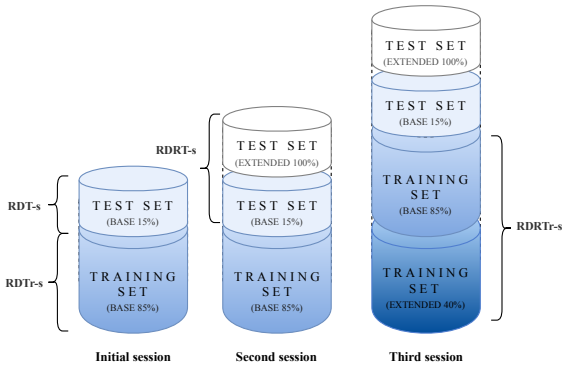

Figure 3: A visualisation of the experimental setup and the dataset split for each test session. Where the original percentage represents the initial split of the dataset, while the extended percentage illustrates the percentual increase of the test set and training set, respectively. The test is divided in three sessions, where the first provides the base accuracy, the second the robustness after exposure to variations and the third will yield result of robustness after inducing variation in the training data.

4 EXPERIMENTAL SETUP

Three test sessions were performed to establish a base accuracy, a robustness accuracy, and an enhanced accuracy. The setup of the three tests can be viewed in Fig. 3. Each test was executed under equal conditions to be able to compare the result from one session to another. All variables, such as architecture, backbone, batch size, computational power, iterations, and learning rate had to be consequent for the three test sessions.

Weather augmentations as well as synthesised images both contains artificial artefacts, which could be interpreted differently by the object detector compared to actual weather conditions or presence of objects. Furthermore, synthesised images suffers from another dilemma with respect to artificial elements - artificially induced objects are most likely to lack in context-awareness. One or more parameters, such as scale, position, rotation, and reflections of light, is likely to be inaccurate with respect to the background image. Therefore the amount of artificial artefacts induced to the images were measured using Natural Image Quality Evaluator (NIQE) (Mittal et al., 2012), a quality index measuring tool.

4.1 Experiment

The experiments are divided into three stages, a preparation phase, followed by a training phase, and an evaluation phase constructed in three test sessions. Faster R-CNN was used as the architecture framework during the entire experiment. ResNeXt-101-FPN, Resnet-101-FPN, and ResNet-50-FPN were evaluated as a backbone during the initial test session. Based on the results, ResNet-50-FPN was applied as a backbone during the second and third test sessions.

4.1.1 Preparation Phase

The images were extracted from in-flight videos over an airport. To supplement these, royalty-free images with relevant motifs were gathered. Environment, object scale, resolution, climate, and colour of images were disregarded during collection. Keywords applied during search and collection of royalty-free images: *Aerial view of airport*, *Aircraft*, *Airfield*, *Airport*, *Airport from above*, *Airport ground vehicle*, *Airstrip*, *Car*, *Flight*, *Helicopter*, *Runway*, *Truck*, and *Truck at airport*.

The Initial Session. Altogether, 2318 distinct images were at hand. The base dataset with no data augmentation is used for the initial test session, determining the base accuracy. Therefore, a subset of the base dataset was augmented to extend the number of images available for training and test resulting in 3318 images for the base dataset. The Python library Imgaug[1] provided the augmentation techniques necessary for the base dataset as well as for the second and third test session; each category applied can be seen in Table 1. The first six categories were applied to extend the base dataset. Python's pseudo-random library Random was used to single out which images to augment, to avoid inflicting any bias. Likewise, the same method was used to determine the number of augmentation techniques to be applied for each single image, as well as which technique(s). At most three different techniques were applied to a single image, at minimum one technique. Every 3318 images of the base dataset were arranged into one of two sets, referred to as Runway Detection Training set (RDTr-s) and Runway Detection Test set (RDT-s). The images were split into folders of similar size, each folder was then pseudo-randomly classified as either training or test close to the percentage 85/15. RDTr-s consisted of 2795 images, RDT-s of 523.

The Second Session. For the second test session, a second test set was utilised - Runway Detection Robust Test set (RDRT-s). To create the second test set, all images of the first test set RDT-s were augmented using the augmentation techniques of the last four categories in Table 1. The augmentation was performed in the same manner as the augmentation of the base set to avoid inflicting any bias. A second approach, synthesising, was included in addition to augmenta-

[1] https://github.com/aleju/imgaug

Table 1: Categorising augmentation methods used to produce the augmented images. First six categories were allocated to create RDTr-s and RDT-s, while the remaining categories where used to create RDRTr-s and RDRT-s.

Category	Augmentation	Setting	Unit
Colour	Grayscale	alpha=(0.0, 1.0)	Percent
	Remove saturation	-	Percent
	Change colour temperature	(2000, 16000)	Kelvin
Contrast	Gamma contrast	(0.5, 2.0)	Pixel value per channel
	All channels CLAHE (Contrast Limited Adaptive Histogram Equalisation)	-	Channel by channel normalisation
Convolutional	Edge detect	alpha=(0.0, 1.0)	Percent
Flip	Fliplr	-	Percent to flip
	Flipud	-	Percent to flip
Geometric	Perspective transform	scale=(0.01, 0.15)	Distance to image corner points
	Rotate	(-45, 45)	Degree(s)
Size	Crop	px=(1, 16)	Pixel(s)
Arithmetic	Add	(-40, 40)	Pixel value addition term
	Multiply	(0.5, 1.5), per_channel=0.5	Pixel value multiplication factor, percent channel-wise
	Cutout	nb_iterations=(1, 3)	Quantity of rectangular(s)
Blur	Gaussian blur	sigma=(0.0, 3.0)	Variance
	Motion blur	k=15	Kernel size
Corruption	Snow	severity=random.randint(1, 5)	Severity level
	Motion blur	severity=random.randint(1, 5)	Severity level
	brightness	severity=random.randint(1, 5)	Severity level
Weather	Fog	-	-
	Clouds	-	-
	Rain	-	-
	FastSnowyLandscape	lightness_threshold=(130, 200)/ lightness_threshold=[100, 120], lightness_multiplier=(2.3, 2.7)	Pixel value threshold

tion to enrich the dataset with relevant objects. Objects covered by the classes were masked out from the royalty-free images with approval for modification, 30 objects were extracted in total. Images from the base dataset were used as background. Each object was manually added as the foreground layer to one of the background images. This generated 24 synthesised images, all of whom were also augmented to generate 144 synthesised images in total. Plus, 72 images were added to the second test set RDRT-s.

The Third Session. A second training set was to be utilised for the third test session - Runway Detection Robust Training set (RDRTr-s). The remaining synthesised images, 72 images, were added to the second training set together with another 1000 images generated by augmentation. Approximately 36% of the first training set RDTr-s was pseudo-randomly selected and augmented using the same augmentation techniques as for the second test set RDRT-s. Half of the synthesised images, the first training set, and the 1000 augmented images, made up the second training set. An example of the synthesised images is illustrated in Fig. 4, weather and lighting augmentations in Fig. 5.

Table 2: The created datasets, divided by name and number of images in each set. Last column represents which test session the corresponding datasets where utilised, S1 for the initial session, S2 for the second session, and S3 for the third session.

Dataset	Size	Applied
Runway Detection Training set (RDTr-s)	2795 images	S1, S2
Runway Detection Test set (RDT-s)	523 images	S1
Runway Detection Robust Training set (RDRTr-s)	3866 images	S3
Runway Detection Robust Test set (RDRT-s)	1088 images	S2, S3

In Table 2 all four sets are presented with their respective size. Amount of annotations for each set and class can be seen in Table 3, average annotations per image for each set and class can be seen in Table 4. LabelImg (Tzutalin, 2015) was used to annotate the images of the four datasets. All objects which fell under the classes 'Aircraft', 'Car', 'Helicopter', 'Human', 'Runway', and 'Truck' were annotated. However, 'Car' and 'Truck' was at a later stage merged to one class 'Vehicle'. Prior to annotation, the images' resolution was not considered, but due to graphical

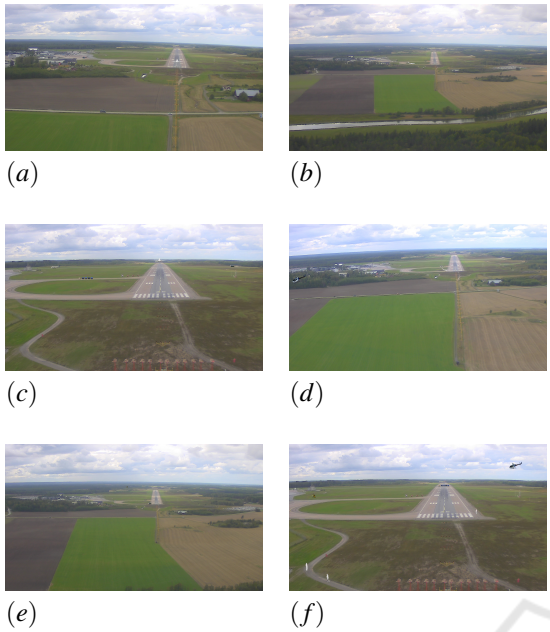

Figure 4: Example of created synthesised images used within RDRTr-s and RDRT-s. (a) Aircraft(1) and Helicopter(1) synthesised (b) Aircraft(2) synthesised (c) Aircraft(1) and Vehicle(2) synthesised (d) Aircraft(1), Helicopter(1), and Vehicle(1) synthesised (e) Helicopter(1) and Vehicle(2) synthesised (f) Aircraft(1), Helicopter(2), Human(3), and Vehicle(1) synthesised.

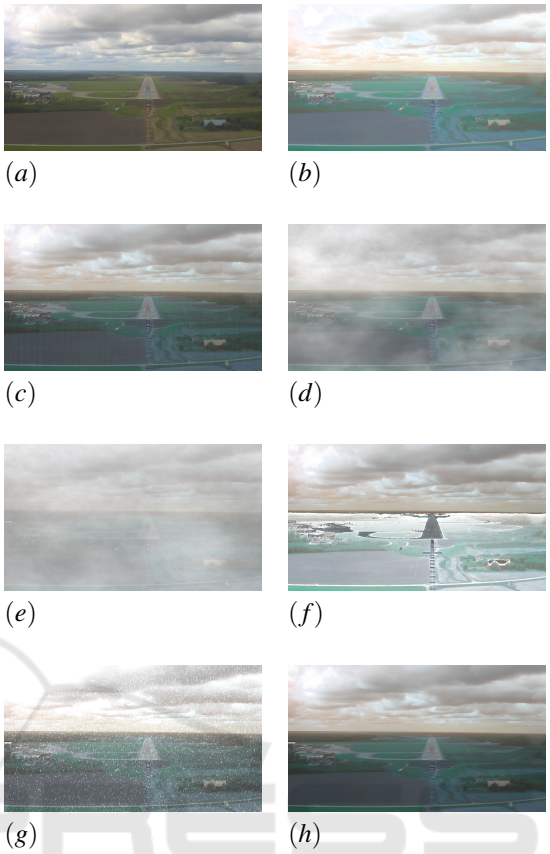

Figure 5: Examples of augmentation applied on original images for the robust training and test sets, with setting specified in Table 1. (a) Original image (b) Brightness (c) Rain (d) Clouds (e) Fog (f) Fast Snowy Landscape (g) Snow (h) Motion Blur, Blur.

memory restrictions, a generic resolution of all images was required. Therefore, all images were resized to the highest generic resolution possible without triggering a CUDA out of memory alert, 600×400 pixels. Since this was conducted after completing the annotations, all annotation coordinates were re-scaled by the same factor, as presented by Equation 1.

$$newCord_{x/y/min/max} = orgCord_{x/y/min/max} \times \frac{newRes_{x/y}}{oldRes_{x/y}} \quad (1)$$

4.1.2 Training Phase

For the experiment, two training sessions were executed, to complete the initial test session and the third test session. The Detectron2 (Wu et al., 2019) development framework was used to achieve a **.pth-file* with weights, training parameters, scheduler dictionary, and optimiser dictionary. Basically the development framework is intended for development within a Linux environment, to allow the training to run in a Windows environment variables in the Pytorch build[2] had to be made. To enable accelerated training, the framework was compiled with CUDA[3]. Hyperparameters which control the training characteristics in Detectron2 are epochs, batch size per image, number of classes, and learning rate. The number of epochs completed is determined by the number of iterations. Amount of images present in the training set and batch size determines the number of iterations equal to completing one epoch, in accordance with Equation (2). All settings modified during the experiment can be viewed in Table 5.

$$\text{Iterations per epoch} = \frac{\text{Number of images}}{\text{Images per batch}} \quad (2)$$

At the beginning of a training session the learning rate can either be fixed, start at high value and thereafter decline, or gradually increase until reaching a ceiling (the base learning rate). If applying the latter, the warm-up iterations determine at which point

[2]https://github.com/conansherry/detectron2

[3]https://www.nvidia.com/object/io_69526.html

Table 3: Compilation of the total number of annotated instances, total and class wise, for each dataset.

Dataset	Total annotation instances	$\text{Class}_{Aircraft}$ annotation instances	Class_{Runway} annotation instances	$\text{Class}_{Vehicle}$ annotation instances	$\text{Class}_{Helicopter}$ annotation instances	Class_{Human} annotation instances
RDTr-s	17453	4451	1247	8979	301	2475
RDT-s	3670	1098	121	1815	37	599
RDRTr-s	23306	5858	1708	11938	507	3295
RDRT-s	7062	2102	300	3468	89	1103

Table 4: Average number of annotation instances per image, total and class wise, for each dataset.

Dataset	Average annotation instances per image	$\text{Class}_{Aircraft}$ Average annotation instances per image	Class_{Runway} Average annotation instances per image	$\text{Class}_{Vehicle}$ Average annotation instances per image	$\text{Class}_{Helicopter}$ Average annotation instances per image	Class_{Human} Average annotation instances per image
RDTr-s	6.2	1.6	0.4	3.2	0.1	0.9
RDT-s	7.0	2.1	0.2	3.5	0.07	1.1
RDRTr-s	6.0	1.5	0.4	3.1	0.1	0.9
RDRT-s	6.5	1.9	0.3	3.2	0.08	1.0

Table 5: Overview of parameter settings during training with RDTR-s. a) Cyclic learning rate settings. b) Exponential cyclic learning rate setting. Solution b) used in final implementation.

Parameter	**Value**
Number of workers	2
Images per batch	2
Batch size per image	256
Number of iterations	9088
Number of classes	5
Warm-up method	'Linear'
Warm-up iterations	4544
Base learning rate	a) 0.006
	b) 0.006, 0.00589, 0.00555, 0.005007, 0.00424, 0.003243
Gamma, γ	a) 0.9618
	b) 0.9618, 0.9614, 0.9626, 0.9648, 0.9684, 0.9742
Steps	4545, 4645, 4745, 4845, 4945, 5045, 5145, 5245, 5345, 5445, 5545, 5645, 5745, 5845, 5945, 6045, 6145, 6245, 6345, 6445, 6545, 6645, 6745, 6845, 6945, 7045, 7145, 7245, 7345, 7445, 7545, 7645, 7745, 7845, 7945, 8045, 8145, 8245, 8345, 8445, 8545, 8645, 8745, 8845, 8945, 9045,

the learning rate will cease to increase, i.e. when the base learning rate shall be reached. For each defined step after the warm-up period the learning rate will be decreased by gamma, γ. Research of optimal learning rates are ongoing, L. N. Smith (Smith, 2017) presented cyclic learning rate as a method attempting to achieve higher accuracy while decreasing training time. During this experiment, the method was mimicked, with 0.001 as the lowest and 0.006 highest learning rate (base learning rate). Additionally, an exponential decrease of the learning rate was applied after every cycle. To achieve the exponential decline, the base learning rate and the gamma value had to be updated regularly. The base learning rate of every cycle was determined by interpolating an exponential function between the initial base learning rate, 0.006, and the minimum learning rate, 0.001, over a defined interval of iterations. Half a cycle was set to 4544 iterations and 9088 iterations as full cycle length. A graph of the exponential function is visualised in Fig. 6, where the blue points represents the base learning rate for each cycle. As a result, the base learning rate follows Equation (3), where x is number of iterations,

$$\begin{aligned} base_{lr} &= -1.1e^{-12}x^2 + 0.006 \\ x &\in 4544 \leq i \leq 49948 \end{aligned} \tag{3}$$

The gamma value was updated for every cycle according to Equation (4), where min_{lr} is the minimum learning rate and $base_{lr}$ is the base learning rate.

$$\gamma = \sqrt[45]{\frac{min_{lr}}{base_{lr}}}, \tag{4}$$

Neither a cyclic learning rate nor an exponential learning rate is currently supported by the Detectron2 development framework. This is due to an internal scheduler dictionary, `'WarmupMultiStepLR'` the default scheduler of Detectron2, which holds last recorded parameter values. The last recorded learning rate together with iterations, γ, and steps, are loaded prior to a new training cycle. Therefore, the scheduler

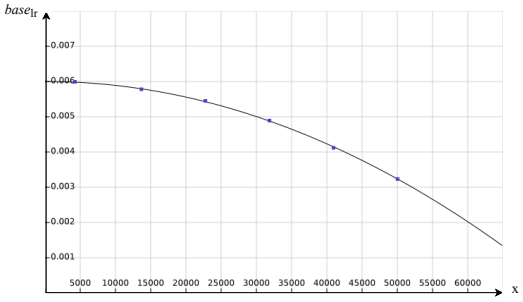

Figure 6: A function of the base learning rate, where x-axis corresponds to the number of iterations and y-axis is $base_{lr}$.

dictionary was overwritten every cycle to achieve the desired behaviour.

Implementation Details. All four custom datasets, RDTr-s, RDT-s, RDRTr-s, and RDRT-s, were registered through the data loader of Detectron2 which utilises Pytorch[4] to read the image and JSON files. Training metrics, loss, class accuracy, false-negatives, and foreground accuracy, are recorded and written to event files during training while a .pth-file is produced at the end of training. The .pth-file, on the other hand, can be used to re-load the training from the last saved checkpoint. For the third test session, the second training session, the .pth-file from the first training session was re-loaded to use the pre-trained model's weights.

5 RESULTS

All gathered results from the three test suits of the experiment are presented within this section. All tables combined covers achieved accuracy scores and measured average quality index for the original-, augmented-, and synthesised images. A qualitative detection capability comparison between second and third session is presented in Section 5.3.

5.1 First Test Session

Faster R-CNN, as the most accurate architecture on Pascal VOC dataset (Zhao et al., 2019), is selected with three different backbones (ResNeXt-101-FPN, ResNet-101-FPN, and ResNet-50-FPN) for the experiments. The main reason of using Faster R-CNN, as a two-stage detector, is that one-stage detectors, such as YOLO (Redmon et al., 2016) and SSD (Liu et al., 2016), have poor localisation accuracy of small objects (Levin and Vidimlic, 2020). Although one-stage detectors have a faster detection speed, efficient inference time is not the priority of the safety-critical auto-landing application (Forsberg et al., 2020).

Base accuracy scores with each backbone trained on RDTr-s and tested on RDT-s can be seen in Table 6. During the larger part of all conducted training cycles, the accuracy of each cycle was measured. In total six training cycles were performed for each backbone, and the measured accuracy can be viewed in Table 7. Measured accuracy scores of 'Car', 'Truck', and 'Vehicle' are presented in Table 8and the class accuracy of each backbone is shown in Table 9.

5.2 Second and Third Test Session

A quality index, NIQE (Mittal et al., 2012), was used to measure the induced error by artificial artefacts in the augmented and synthesised images. To allow for any conclusions to be made, the original images were also evaluated to achieve a reference value for the altered images. An average quality index for each image class is presented in Table 10. The result indicates the augmented images to be furthest from reality, yet not drastically deteriorated from the original images, with a score increment of 0.9801. For the second and third test session, Faster R-CNN was used as architecture framework and ResNet-50-FPN as backbone. Choice of backbone was based on the achieved accuracy scores of the first test session (Table 6). The obtained accuracy for the second and third test session can be viewed in Table 11. According to the table 6, we improve the accuracy 2% on average. Additionally, the class accuracy scores achieved during the second and third test session are presented in Table 12. The accuracy scores of the second test session were gathered by reusing the object detection model trained with RDTr-s to run a test with the RDRT-s. While the accuracy scores of the third test session were achieved by training an object detection model with RDRTr-s and thereafter running a test with the RDRT-s.

5.3 Quantitative Results

The detection capability between the second and third test session was measured and compared, by observing the confidence output for each detected object as well as the number of objects detected. The confidence output for each identified object is given in percentage, representing the certainty level for an object belonging to one of the the chosen classes (Figure 7).

[4]https://pytorch.org/docs/stable/torchvision/datasets.html

Table 6: Top accuracy score over 39 training epochs for the first test session with three different backbone networks.

Test session	Object detection	RDT-s (AP@[IoU= .5:.95])%	RDT-s (AP IoU=.5) %	RDT-s (AP IoU=.75) %	RDT-s (AP_{small}) %	RDT-s (AP_{medium}) %	RDT-s (AP_{large}) %
1	Faster R-CNN w. ResNet-50-FPN	50.327	81.108	54.534	37.004	62.852	70.363
1	Faster R-CNN w. ResNet-101-FPN	48.687	80.792	50.551	35.096	62.671	71.126
1	Faster R-CNN w. ResNeXt-101-FPN	46.692	82.294	44.690	40.231	56.999	67.269

Table 7: Accuracy results of the first test session for Faster R-CNN with the three different backbone networks. Results given in *AP@[IoU=.5:.95] %* score over each training cycle with RDTr-s. The three backbone networks were trained during the same amount of cycles, however some documented data results were lost after completed training.

Test Session	Object detection	1st Cycle	2nd Cycle	3rd Cycle	4th Cycle	5th Cycle	6th Cycle
1	Faster R-CNN w. ResNet-50-FPN	47.794	50.327	48.530	49.225	49.678	49.668
1	Faster R-CNN w. ResNet-101-FPN	48.687	-	-	-	-	-
1	Faster R-CNN w. ResNeXt-101-FPN	-	46.450	45.253	46.692	-	-

Table 8: The top accuracy score over 39 training epochs for the first test session from class 'Vehicle' split in two sub-classes, 'Car' and 'Truck', and result from combined class 'Vehicle' for Faster R-CNN with ResNeXt-101-FPN backbone with RDT-s.

Test session	Object detection	RDT-s $Class_{Car}$%	RDT-s $Class_{Truck}$%	RDT-s $Class_{Vehicle}$%
1	Faster R-CNN w. ResNet-50-FPN	-	-	38.368
1	Faster R-CNN w. ResNet-101-FPN	-	-	33.810
1	Faster R-CNN w. ResNeXT-101-FPN	11.906	45.069	38.442

Table 9: Top accuracy score over 39 training epochs for Faster R-CNN with three different backbones with RDT-s.

Test session	Object detection	RDT-s $Class_{Aircraft}$ %	RDT-s $Class_{Human}$ %	RDT-s $Class_{Vehicle}$ %	RDT-s $Class_{Runway}$ %	RDT-s $Class_{Helicopter}$ %
1	Faster R-CNN w. ResNet-50-FPN	58.802	54.854	38.368	69.019	42.549
1	Faster R-CNN w. ResNet-101-FPN	57.172	52.593	33.810	69.616	45.120
1	Faster R-CNN w. ResNeXt-101-FPN	57.322	30.336	38.442	76.104	31.147

Table 10: Obtained average quality index for original-, augmented-, and synthesised images.

Image representation	Average Quality Index NIQE
Original	2.6071
Augmented	3.5872
Artificially induced objects	2.8068

6 DISCUSSION

In this section, the key ideas and findings during the research are discussed.

6.1 Custom Dataset

The largest part of this work, and it's most valuable resulted product, is the four datasets of the operational environment. Producing enough images for each dataset required gathering, augmentation, and synthesising of images while simultaneously minimising any risk of bias. Besides, the annotation process following the collection of images was very time consuming due to feature-rich images. For example, the annotation of the base dataset took two weeks for two people to complete. Despite feature-rich images the datasets had unbalanced distributions of object classes, some classes were more represented than

Table 11: Top accuracy score over 39 training epochs for the second and third test sessions.

Test session	Object detection	RDRT-s (AP@[IoU= .5:.95])%	RDRT-s (AP IoU=.5) %	RDRT-s (AP IoU=.75) %	RDRT-s (AP_{small}) %	RDRT-s (AP_{medium}) %	RDRT-s (AP_{large}) %
2	Faster R-CNN w. ResNet-50-FPN	32.18	59.327	32.390	28.672	34.079	48.345
3	Faster R-CNN w. ResNet-50-FPN	47.738	78.835	51.180	41.392	53.288	61.832

Table 12: Top accuracy score for each class over 39 training epochs for the second and third test sessions.

Test session	Object detection	RDRT-s $Class_{Aircraft}$ %	RDRT-s $Class_{Human}$ %	RDRT-s $Class_{Vehicle}$ %	RDRT-s $Class_{Runway}$ %	RDRT-s $Class_{Helicopter}$ %
2	Faster R-CNN w. ResNet-50-FPN	42.674	20.283	24.306	56.528	17.145
3	Faster R-CNN w. ResNet-50-FPN	55.689	31.474	43.282	67.661	40.584

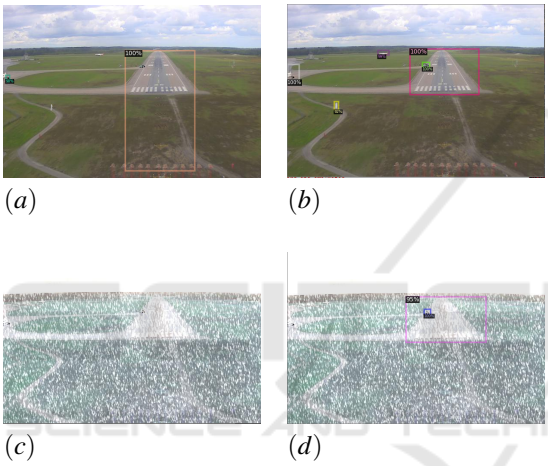

Figure 7: Comparison of object detection results with weather and lighting augmentations in training dataset (b and d) and without augmentation (a and c). (a) Synthesised image: Vehicle(90 %) falsely detected and Runway(100 %) detected, one aircraft, one human, and one vehicle undetected, (b) Synthesised image: Aircraft(100 %, 99 %), Runway(100 %), Human(92 %), (c) Snow augmentation: Two aircraft, one human, and one vehicle undetected, (d) Snow augmentation: Runway(95 %) and Vehicle(100 %) detected, two aircraft and one human undetected.

others. Due to the number of certain objects covered by royalty-free images, the class 'Helicopter' was by far underrepresented. In contrast, the class 'Vehicle' covered both common objects, car and truck, which led to an over representation. The uneven distribution was reduced during augmentation, however not equal, thus adding new images to the datasets is beneficial.

6.2 Development Framework

Custom datasets generally entail hold-ups during the development of deep learning-based object detection models but are a requirement for usage within safety-critical applications since they highly affect the performance of the final model. Therefore, it was necessary with an efficient development framework to stay within the schedule, for this work, the development was performed using Detectron2. The framework allowed for efficient tailoring of training and test sessions; however, low-level customisation options were limited. Yet, the exponential cyclic learning rate was achievable by manually interfering with the scheduler logic. All training sessions were completed using the architecture framework Faster R-CNN. All accuracy scores were logged during the first test session to enable a comparison between the three backbones including ResNeXt-101-FPN, ResNet-101-FPN, and ResNet-50-FPN object CNN models.

6.3 Accuracy Score for Backbone

During research ResNeXt-101-FPN seemed to be the most prominent backbone for this work, surprisingly enough ResNet-50-FPN had the highest performance out of the three and was therefore used throughout the rest of the test sessions. The reason for a better performance of ResNet-50-FPN and the low increase of AP@[IoU=.5:.95] score between the cycles for all three backbones was speculated to be the cause of dying Rectified Linear Unit (ReLU), when no response is given on input by the artificial neurons of the NN. Another explanation for the performance of the three models could be the exponential cycling learning rate. The motivation for using the tailored learning rate was due to higher accuracy in combination with less required training time; this could indicate that the maximum accuracy score achievable with the custom dataset is just slightly above 50. Furthermore, as previously mentioned, all images were resized to a generic size after the annotation process. Most likely,

this resulted in some small objects being in fact too small for the new resolution.

6.4 Effect of Image Enhancement

By analysing the class accuracy achieved during the first test session, it is possible to see a lower performance of class 'Human' and 'Helicopter', especially with ResNeXt-101-FPN. Overall, objects which were more consistent with respect to appearance and size tended to score higher. Class 'Vehicle' had a large variation in both appearance and size since the class covered both cars as well as trucks. While the class 'Human' mostly varied in appearance due to shifting body positions. A significant stagnation of accuracy compared to the first test was recorded during the second test, despite slim differences measured with NIQE between the original images and both the augmented and synthesised images, which points to the modified images not being too far away from reality, increasing the probability of results to be relevant for operation within real-world scenarios. While introducing both the augmented as well as the synthesised images into the training set yielded a significant increase of accuracy, close to the initial accuracy achieved with no corruptions present in the test set. The results indicated corruptions within training data to increase the robustness of the model towards various variations in general.

7 CONCLUSION

The aim of this work was to evaluate if augmentation of weather and luminance in combination with the introduction of artificial artefacts could improve the representation of an operational aircraft environment. By merging the augmented and synthesised images, a robust training dataset could be constructed. The calculated estimation of inducted error by augmentations and artificial artefacts, NIQE score, showed an increased error of 0.2 on average for synthesised images and 0.8 for augmented images. As evident by the results, synthesised images display the closes resemblance with the original images. However, augmented images are not drastically deteriorated, which indicate that the dataset has a close resemblance to the real operational environment. Introducing variations in the constructed dataset yielded an improvement of prediction accuracy by a factor of 1.48 for AP@[IoU=.5:.95], from 32.187 (%) to 47.738 (%) and by a factor of 1.33, from 59.327 (%) to 78.835 (%) for IoU=.5, when comparing to the second test session. By extending the dataset with the representation of variation in the environment, the robustness is improved to maintain accuracy.

ACKNOWLEDGEMENT

We wish to express our gratitude towards SAAB for providing us the experimental dataset. A sincere appreciation to Per-Olof Jacobson for valuable guidance and providing us resources throughout the work. This Paper is supported by Knowledge Foundation (KKS) within DPAC and DeepMaker projects.

REFERENCES

Alam, M. S., Ashwin, T., and Reddy, G. R. M. (2020). Optimized object detection technique in video surveillance system using depth images. In *Smart Computing Paradigms: New Progresses and Challenges*, pages 19–27. Springer.

Association, I. A. T. et al. (2019). Iata safety report 2019. *Montreal, Canada*.

Badue, C., Guidolini, R., Carneiro, R. V., Azevedo, P., Cardoso, V. B., Forechi, A., Jesus, L., Berriel, R., Paixão, T., Mutz, F., et al. (2019). Self-driving cars: A survey. *arXiv preprint arXiv:1901.04407*.

Ball, D., Upcroft, B., Wyeth, G., Corke, P., English, A., Ross, P., Patten, T., Fitch, R., Sukkarieh, S., and Bate, A. (2016). Vision-based obstacle detection and navigation for an agricultural robot. *Journal of field robotics*, 33(8):1107–1130.

Burton, S., Gauerhof, L., and Heinzemann, C. (2017). Making the case for safety of machine learning in highly automated driving. In *International Conference on Computer Safety, Reliability, and Security*, pages 5–16. Springer.

Dave, G., Chao, X., and Sriadibhatla, K. (2010). Face recognition in mobile phones. *Department of Electrical Engineering Stanford University, USA*, pages 7–23.

Deng, J., Dong, W., Socher, R., Li, L.-J., Li, K., and Fei-Fei, L. (2009). Imagenet: A large-scale hierarchical image database. In *2009 IEEE conference on computer vision and pattern recognition*, pages 248–255. Ieee.

Engelcke, M., Rao, D., Wang, D. Z., Tong, C. H., and Posner, I. (2017). Vote3deep: Fast object detection in 3d point clouds using efficient convolutional neural networks. In *2017 IEEE International Conference on Robotics and Automation (ICRA)*, pages 1355–1361. IEEE.

Everingham, M., Van Gool, L., Williams, C. K., Winn, J., and Zisserman, A. (2010). The pascal visual object classes (voc) challenge. *International journal of computer vision*, 88(2):303–338.

Faria, J. M. (2017). Non-determinism and failure modes in machine learning. In *2017 IEEE International Symposium on Software Reliability Engineering Workshops (ISSREW)*, pages 310–316. IEEE.

Federal Aviation Administration (2000). Installation of terrain awareness and warning system (taws) approved for part 23 airplanes. accessed: 1 August 2020.

Federal Aviation Administration (2017). Airworthiness approval of traffic alert and collision avoidance systems (tcas ii), versions 7.0 & 7.1 and associated mode s transponders. accessed: 1 August 2020.

Forsberg, H., Lindén, J., Hjorth, J., Månefjord, T., and Daneshtalab, M. (2020). Challenges in using neural networks in safety-critical applications. In *2020 AIAA/IEEE 39th Digital Avionics Systems Conference (DASC)*, pages 1–7. IEEE.

Gatys, L. A., Ecker, A. S., and Bethge, M. (2015). A neural algorithm of artistic style. *arXiv preprint arXiv:1508.06576*.

Geirhos, R., Rubisch, P., Michaelis, C., Bethge, M., Wichmann, F. A., and Brendel, W. (2018). Imagenet-trained cnns are biased towards texture; increasing shape bias improves accuracy and robustness. *arXiv preprint arXiv:1811.12231*.

Geng, H., Guan, J., Pan, H., and Fu, H. (2018). Multiple vehicle detection with different scales in urban surveillance video. In *2018 IEEE Fourth International Conference on Multimedia Big Data (BigMM)*, pages 1–4. IEEE.

Hendrycks, D. and Dietterich, T. G. (2018). Benchmarking neural network robustness to common corruptions and surface variations. *arXiv preprint arXiv:1807.01697*.

ICAO, A. (2019). State of global aviation safety. *Montreal, Canada*.

Inoue, H. (2018). Data augmentation by pairing samples for images classification. *arXiv preprint arXiv:1801.02929*.

J.Steward (2018). Tesla's autopilot was involved in another deadly car crash. accessed: 1 August 2020.

Levin, A. and Vidimlic, N. (2020). Improving situational awareness in aviation: Robust vision-based detection of hazardous objects.

Lin, T.-Y., Maire, M., Belongie, S., Hays, J., Perona, P., Ramanan, D., Dollár, P., and Zitnick, C. L. (2014). Microsoft coco: Common objects in context. In *European conference on computer vision*, pages 740–755. Springer.

Liu, W., Anguelov, D., Erhan, D., Szegedy, C., Reed, S., Fu, C.-Y., and Berg, A. C. (2016). Ssd: Single shot multibox detector. In *European conference on computer vision*, pages 21–37. Springer.

Loni, M., Sinaei, S., Zoljodi, A., Daneshtalab, M., and Sjödin, M. (2020). Deepmaker: A multi-objective optimization framework for deep neural networks in embedded systems. *Microprocessors and Microsystems*, 73:102989.

Michaelis, C., Mitzkus, B., Geirhos, R., Rusak, E., Bringmann, O., Ecker, A. S., Bethge, M., and Brendel, W. (2019). Benchmarking robustness in object detection: Autonomous driving when winter is coming. *arXiv preprint arXiv:1907.07484*.

Mitsa, T. (2019). How Do You Know You Have Enough Training Data? accessed: 1 August 2020.

Mittal, A., Soundararajan, R., and Bovik, A. C. (2012). Making a "completely blind" image quality analyzer. *IEEE Signal Processing Letters*, 20(3):209–212.

O'Mahony, N., Campbell, S., Carvalho, A., Harapanahalli, S., Hernandez, G. V., Krpalkova, L., Riordan, D., and Walsh, J. (2019). Deep learning vs. traditional computer vision. In *Science and Information Conference*, pages 128–144. Springer.

Redmon, J., Divvala, S., Girshick, R., and Farhadi, A. (2016). You only look once: Unified, real-time object detection. In *Proceedings of the IEEE conference on computer vision and pattern recognition*, pages 779–788.

Shorten, C. and Khoshgoftaar, T. M. (2019). A survey on image data augmentation for deep learning. *Journal of Big Data*, 6(1):60.

Skybrary (2017). B744 / vehicle, luxembourg airport, luxembourg 2010. accessed: 1 August 2020.

Smith, L. N. (2017). Cyclical learning rates for training neural networks. In *2017 IEEE Winter Conference on Applications of Computer Vision (WACV)*, pages 464–472. IEEE.

Taylor, L. and Nitschke, G. (2017). Improving deep learning using generic data augmentation. *arXiv preprint arXiv:1708.06020*.

Tzutalin (2015). Labellmg. accessed: 1 August 2020.

Wu, Y., Kirillov, A., Massa, F., Lo, W.-Y., and Girshick, R. (2019). Detectron2.

Zhang, L., Zhai, Z., He, L., Wen, P., and Niu, W. (2019). Infrared-inertial navigation for commercial aircraft precision landing in low visibility and gps-denied environments. *Sensors*, 19(2):408.

Zhao, Z.-Q., Zheng, P., Xu, S.-t., and Wu, X. (2019). Object detection with deep learning: A review. *IEEE transactions on neural networks and learning systems*, 30(11):3212–3232.

Zhong, Z., Zheng, L., Kang, G., Li, S., and Yang, Y. (2017). Random erasing data augmentation. *arXiv preprint arXiv:1708.04896*.